Chinese Chemical Letters 35 (2024) 109506

Contents lists available at ScienceDirect

Chinese Chemical Letters

journal homepage: www.elsevier.com/locate/cclet

Novel berberine derivatives as adjuvants in the battle against *Acinetobacter baumannii*: A promising strategy for combating multi-drug resistance

Liping Zhao[a,1], Xixi Guo[a,1], Zhimeng Zhang[a,1], Xi Lu[a], Qingxuan Zeng[a], Tianyun Fan[a], Xintong Zhang[a], Fenbei Chen[a], Mengyi Xu[a], Min Yuan[b], Zhenjun Li[b], Jiandong Jiang[a], Jing Pang[a,*], Xuefu You[a,*], Yanxiang Wang[a,*], Danqing Song[a,*]

[a] *Beijing Key Laboratory of Antimicrobial Agents, Institute of Medicinal Biotechnology, Chinese Academy of Medical Sciences and Peking Union Medical College, Beijing 100050, China*

[b] *State Key Laboratory for Infectious Diseases Prevention and Control, Collaborative Innovation Center for Diagnosis and Treatment of Infectious Disease, National Institute for Communicable Disease Control and Prevention, Chinese Center for Disease Control and Prevention, Beijing 102206, China*

ARTICLE INFO

Article history:
Received 7 December 2023
Revised 8 January 2024
Accepted 10 January 2024
Available online 14 January 2024

Keywords:
Acinetobacter baumannii
Berberine derivatives
Rational design
Synergistic effect
Efflux
Iron acquisition

ABSTRACT

The development of resistance against most of the available antibiotics has made *Acinetobacter baumannii* (*A. baumannii*) a pathogen of high risk. In this study, thirty novel berberine derivatives are rationally designed, synthesized, and evaluated for their synergistic antibacterial activities against *A. baumannii*. Among them, compound **2d** shows the most potent synergetic effect to aztreonam against *A. baumannii*, including carbapenem-resistant and extended-spectrum β-lactamases-producing strains. Moreover, synergistic effects were observed for the combinations of **2d** and different antibacterial used in clinical practices, indicating its potent broad-spectrum antibiotic-sensitizing effects against *A. baumannii*. The combination of **2d** and aztreonam significantly improves the survival rates of *G. mellonella* larvae compared with aztreonam treatment alone. Mechanism studies indicate that **2d** inhibits the drug efflux and iron acquisition of the bacteria by targeting the AdeB transporter protein, thus achieving a synergistic antimicrobial efficacy with different antibacterial agents. Therefore, berberine derivatives represent a new family of antimicrobial adjuvants against *A. baumannii*, with the advantage of dual-function antibacterial effect, and are worthy of further investigation.

© 2024 Published by Elsevier B.V. on behalf of Chinese Chemical Society and Institute of Materia Medica, Chinese Academy of Medical Sciences.

Acinetobacter baumannii (*A. baumannii*) is a Gram-negative opportunistic nosocomial pathogen, which is responsible for a variety of hospital-acquired and community-acquired infectious diseases, such as pneumonia, urinary tract infections, and surgical site infections, particularly among patients in intensive care units. Drug resistant *A. baumannii*, especially carbapenem-resistant *A. baumannii* (CRAB) has been ranked as the most critical pathogens by World Health Organization (WHO) due to the lack of effective and safe treatment options [1–5]. The development of new antibacterial or antibiotic adjuvants is critically needed. Given the lengthy development cycle for novel antibiotics, exploring novel antibacterial adjuvants to enhance the efficacy of first-line antibiotics is considered as an effective solution for bridging the widening gap between clinical demands and drug innovation. Antibiotic adjuvants, showing little or no antimicrobial activity alone generally [6–10], could enhance antibiotic activity either by blocking resistance or by boosting the host response to infection. Several adjuvants are already in clinical use, such as avibactam, which inhibits the β-lactamases but exhibits no antimicrobial activity alone.

Aztreonam (ATM) is the only monobactam in clinical use, and has been a commonly prescribed antibiotic in clinical practice since 1986, primarily for the treatment of Gram-negative bacterial infections. However, ATM exhibits limited efficacy against *A. baumannii*, mainly due to β-lactamase production and efflux pump overexpression. Berberine (BBR), a traditional Chinese medicine isoquinoline alkaloid, has been used clinically as an antidiarrheal agent for more than 2000 years [11–14], with low general toxicity, genetic toxicity, and mutagenicity *in vitro* and *in vivo*. A moderate synergistic effect between BBR and ATM against *A. baumannii* was demonstrated, which provided further insights for the fu-

* Corresponding authors.
E-mail addresses: pangjing@imb.pumc.edu.cn (J. Pang), xuefuyou@imb.pumc.edu.cn (X. You), wangyanxiang@imb.pumc.edu.cn (Y. Wang), songdanqing@imb.pumc.edu.cn (D. Song).

[1] These authors contributed equally to this work.

https://doi.org/10.1016/j.cclet.2024.109506
1001-8417/© 2024 Published by Elsevier B.V. on behalf of Chinese Chemical Society and Institute of Materia Medica, Chinese Academy of Medical Sciences.

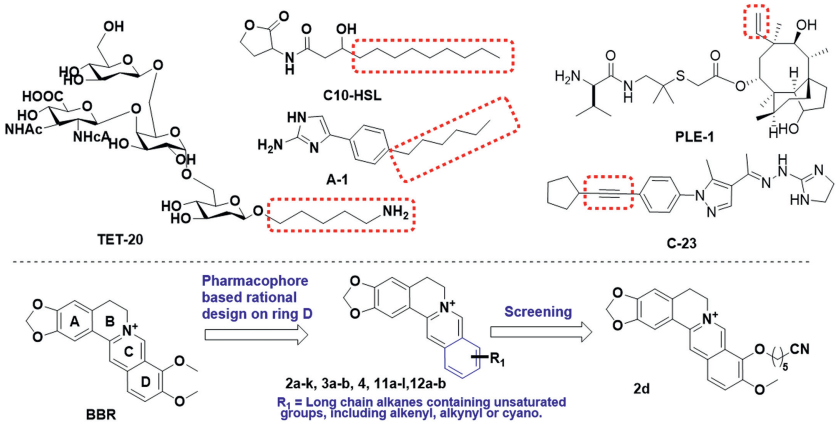

Scheme 1. Chemical structures of antibiotic adjuvants against *A. baumannii*, and structure modification strategy on BBR.

ture development of BBR or its derivatives as an antibiotic adjuvant [15,16]. As of present, there is no literature available regarding the synergistic antibacterial activity of BBR derivatives with antibiotics against *A. baumannii*.

Based on a rational design strategy, we initiated an in-depth structural analysis of the most recently discovered agents exhibiting anti-*A. baumannii* properties or synergistic effects. These synergistic enhancers share a common alkyl chain pharmacophore (Scheme 1), including **C10-HSL** (a quorum sensing inhibitor of *A. baumannii*) [17], compound **A-1** (aminimizole-based small molecule adjuvant suppresses *A. baumannii* resistance by down-regulating the PmrAB system) [18], and an oligosaccharide **TET-20** (a candidate vaccine adjuvant against *A. baumannii*) [19]. Moreover, recently identified novel candidates exhibiting anti-*A. baumannii* properties, such as the pleuromutilin analogue **PLE-1** [20] and the benzopyrazole compound **C-23** [21], feature unsaturated moieties such as alkenyl and alkynyl groups. At present, the reported structural modifications of BBR derivatives with antibacterial activity mainly focus on the ring C or D, and derivatives resulting from C-ring modifications (positions 7, 8, and 13) of BBR typically exhibit enhanced activity against Gram-positive bacteria [22,23]. Conversely, modifications targeting the D-ring (positions 9 and 12) may yield more promising candidates with activity against Gram-negative bacteria [24,25]. Therefore, the structural modifications in this study predominantly focused on the D-ring. These findings serve as a foundation and guidance for subsequent modifications of BBR derivatives.

Herein, based on the summary of pharmacophore which is beneficial to improve anti-*A. baumannii* synergistic activity, thirty novel BBR derivatives with unsaturated moieties containing alkyl chain pharmacophore on ring D were rationally designed and synthesized (Scheme 1). The synthetic route was described in Schemes S1–S3 (Supporting information). The antimicrobial activities of all the newly synthesized compounds used alone and in combination with ATM against *A. baumannii* ATCC 19606, a reference strain commonly used in antibacterial activity evaluation, were evaluated *via* the broth microdilution method and checkerboard analysis, respectively, taking BBR and levofloxacin as the positive controls. The minimum inhibitory concentration (MIC) value of levofloxacin against the ATCC 19606 strain is 0.25 μg/mL (Table S1 in Supporting information), indicating the reliability of the experimental results. The combined effect of all target compounds and ATM were indicated by fractional inhibitory concentration index (FICI). The combination was defined to be synergistic when the FICI was $\leq$0.5; indifferent when $0.5 < \text{FICI} < 4$; antagonistic when $\text{FICI} \geq 4$. The MICs and FICIs of the analogues were listed in Table S1 (Supporting information).

The results showed that BBR exhibited a weak inhibitory effect on *A. baumannii* ATCC 19606 when used alone, with an MIC of 1024 μg/mL. In the case of combination, a synergistic effect was observed, with an FICI of 0.281. The addition of 32 μg/mL BBR led to a significant decrease in the MIC value of ATM from 32 μg/mL to 8 μg/mL. Structure–activity relationship (SAR) study of BBR's derivatives was first focused on the 9-substituents of BBR, and compounds with ether linker (**2a**–**k**) at position 9 were prepared and screened. Out of these compounds, **2a** and **2b**, which feature 1-butynyl and 1-octynyl substituents, respectively, demonstrated superior synergistic effects than BBR, with FICIs of 0.258 and 0.254. When the alkynyl group was replaced by a cyano group, compounds **2c**–**e** were synthesized and evaluated. Compound **2d** exhibited a promising synergistic potency with an FICI value of 0.129. The MIC of ATM against *A. baumannii* was reduced to 4 μg/mL (1/8 MIC) with the addition of only 4 μg/mL **2d**, which was significantly lower than that of BBR (32 μg/mL). Next, compound **2f** in conjunction with an internal alkyne showed comparable activity, compared with BBR. Additionally, compounds **2g** and **2h**, which contained an alkenyl group, displayed improved synergetic effects with the FICI values around 0.25 when compared to the leading compound. Meanwhile, **2i**–**k** with polyethylene glycol linker showed comparable activities to those alkane linker derivatives. An indifferent effect ($\text{FICI} > 0.5$) was observed in the combination of ATM and **3a** or **3b** with a reduced tetrahydroberberine skeleton, suggesting the π-conjugated structure might play a critical role in improving synergistic antimicrobial potency of BBR analogues. Next, 9-amine BBR analogue **4** was generated and only exhibited moderate activity. These findings highlight the favorable effects of appropriate modification at 9-position in optimizing the synergic activities.

When the same substituent groups were moved to position 10, compounds **11a**–**l**, **12a** and **12b** were generated, and they exhibited comparable or decreased activities compared to their counterparts. Among these compounds, **11h** and **11i**, featured alkenyl substituents at position 10, displayed better synergetic effects with the FICIs of 0.254 and 0.252. Similarly, declined synergetic potency of **12a** and **12b** again confirmed the vital role of the conjugated system in improving antimicrobial activity. Finally, a modification was made at the 3-position by selectively opening the methylenedioxy ring to produce compounds **14a** and **14b**. Both compounds exhibited a significant decrease in synergetic activity, indicating that the methylenedioxy moiety in BBR analogues might be essential for synergistic effects. Consequently, six BBR analogues with the best synergistic antibacterial effects, namely **2b**, **2d**, **2g**, **2h**, **11h** and **11i** were selected as the representative compounds for further investigation.

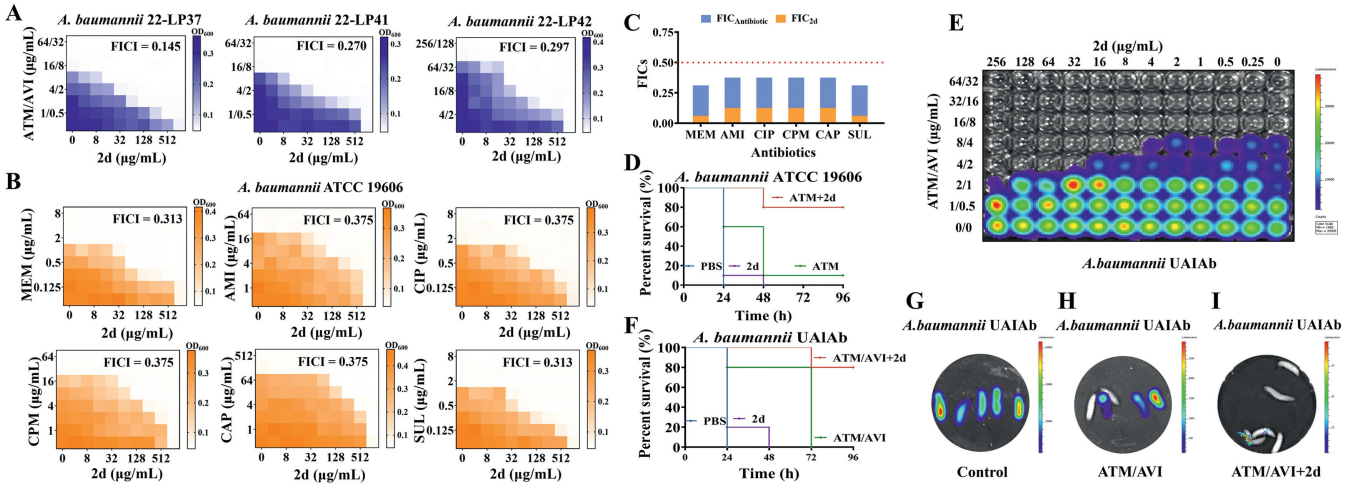

Fig. 1. Synergistic antibacterial effects *in vitro* and *in vivo* for **2d** against *A. baumannii*. (A) Heat map for the antibacterial activity of **2d** in combination with ATM/AVI in ESBL-producing *A. baumannii* 22-LP37, 22-LP41 and 22-LP42 in checkerboard assay. (B) Heat map for the antibacterial activity of **2d** in combination with MEM, AMI, CIP, CPM, CAP and SUL against *A. baumannii* ATCC 19606 in checkerboard assay. (C) Bar chart representing the FICI values of **2d** in combination with MEM, AMI, CIP, CPM, CAP and SUL against *A. baumannii* ATCC 19606. The red dash line delineates the cut-off of synergy with an FICI of 0.5. (D) Survival curves of *G. mellonella* larvae following the infection of *A. baumannii* ATCC 19606 and the treatment of PBS, **2d**, ATM or **2d**/ATM combination ($n = 10$). (E) Checkerboard assay of **2d** with ATM/AVI against autoluminescent *A. baumannii* strain UAIAb. (F) Survival curves of *G. mellonella* larvae following the infection of *A. baumannii* strain UAIAb and the treatment of PBS, **2d**, ATM or **2d**/ATM combination ($n = 5$). Luminescence images of *G. mellonella* larvae ($n = 5$) collected 24 h following the infection of autoluminescent *A. baumannii* strain UAIAb and the treatment of (G) PBS, (H) ATM/AVI or (I) **2d**/ATM/AVI combination.

Six highly active compounds **2b**, **2d**, **2g**, **2h**, **11h** and **11i** were first evaluated for their safety profiles. The MTT assay was used to assess the *in vitro* cytotoxic effects of these compounds on human large cell lung carcinoma cells H460, human hepatocarcinoma cells HepG2, and human acute monocytic leukemia cells THP1. As shown in Table S2 (Supporting information), compound **2d** showed the highest biosafety, with 50% cytotoxicity concentrations (CC_{50}) values of 107.8, 87.75 and 82.45 μmol/L for H460, HepG2 and THP1, respectively. Other compounds containing alkynyl and alkenyl group, including **2b**, **2g**, **2h**, **11h** and **11i**, displayed relatively higher cytotoxicity. Therefore, compound **2d** was chosen as the representative compound for the further investigation.

To preliminarily investigate the pharmacokinetic properties of **2d**, the stability assay was performed in human plasma (Bioreclamation IVT, Cat. No. HUMANPLK2P2N, Batch No. HMN761043) *in vitro* using propantheline bromide, which contains an ester bond, as the control [26]. Compound **2d** and propantheline were incubated with human plasma, and samples were collected at 0, 10, 30, 60, and 120 min, respectively. As shown in Table S3 (Supporting information), propantheline was rapidly hydrolyzed in blood within 1 h, as expected. In contrast, compound **2d** demonstrated satisfactory stability in plasma, remaining stable for up to 2 h.

To explore whether **2d** could enhance the activity of ATM against other *A. baumannii* strains, one standard strain (ATCC 17978) and thirteen randomly selected clinical isolates, including six carbapenem-susceptible strains and seven carbapenem-resistant *A. baumannii* strains were used to conduct the checkerboard assay. As shown in Table S4 (Supporting information), the combination of **2d** and ATM exhibited a synergistic effect against 11 out of 14 tested *A. baumannii* strains, with a median FICI of 0.313. The MIC values of ATM against ATCC 17978, 20-6, 21-22 and 21-24 were reduced to 2–4 μg/mL when used in combination with different concentrations of **2d**. The CRAB isolates demonstrated higher resistance to ATM (MICs at 64–128 μg/mL) compared to *A. baumannii* ATCC 19606. Synergistic effects were also observed in the combination of **2d** and ATM for all the tested CRAB strains, with FICI values ranging from 0.281 to 0.313. These results suggested that the addition of **2d** increased the susceptibility of CRAB strains to ATM. We further evaluated the synergistic effects of the **2d**/ATM combination against three strains of extended-spectrum β-lactamases (ESBLs)-producing *A. baumannii*, including 22-LP37, 22-LP41 and 22-LP42 strains (Table S5 in Supporting information). The FICIs ranged from 0.516 to 0.531, indicating no apparent synergies, which can be explained by the hydrolysis of ATM by ESBLs. Therefore, we continued to explore whether the introducing of β-lactamase inhibitor could restore the synergy of **2d** to ATM against ESBL-producing *A. baumannii*.

Avibactam (AVI) is a non-β-lactam β-lactamase inhibitor that can inhibit almost all serine β-lactamases (SBLs) but not metallo-β-lactamases (MBLs). Due to its stability against MBLs, the ATM-AVI combination may therefore be a viable choice against carbapenem-resistant *Enterobacteriaceae* (CRE) producing SBLs, MBLs, and both. Large-scale *in vitro* susceptibility studies have provided substantial evidence for this strategy, and this combination is actively undergoing clinical development for the treatment of serious infections caused by CRE. However, it has been noted that this approach still exhibits limited potencies against *A. baumannii*. Therefore, the *in vitro* synergistic antibacterial activity of **2d** was evaluated with ATM/AVI against the above mentioned ESBL-producing *A. baumannii* (22-LP37, 22-LP41 and 22-LP42). The results shown in Fig. 1A and Table S6 (Supporting information) indicated that the combination of **2d** (16–32 μg/mL) with ATM/AVI (2:1, concentration ratio) consistently resulted in significantly synergistic effect, with the triple-combination FICIs of 0.145, 0.270 and 0.297 in the three clinical isolates. Considering that ATM is not easily hydrolyzed by MBLs, **2d**/ATM/AVI triple-combination is anticipated to be stable to all classes of β-lactamase, and thus, may provide a promising antibacterial effect against β-lactamase producing *A. baumannii*.

To further explore the synergistic effects of compound **2d** in combination with other antibacterial agents, this study investigated the antimicrobial activity of **2d** in combination with several representative antibacterial of different classes commonly used for clinical treatment of *A. baumannii* infections, including meropenem (MEM), amikacin (AMI), ciprofloxacin (CIP), cefepime (CPM) and chloramphenicol (CAP). Additionally, a β-lactamase inhibitor sulbactam (SUL), which has demonstrated clinical efficacy against *A. baumannii*, was also selected. As shown in Figs. 1B and C, com-

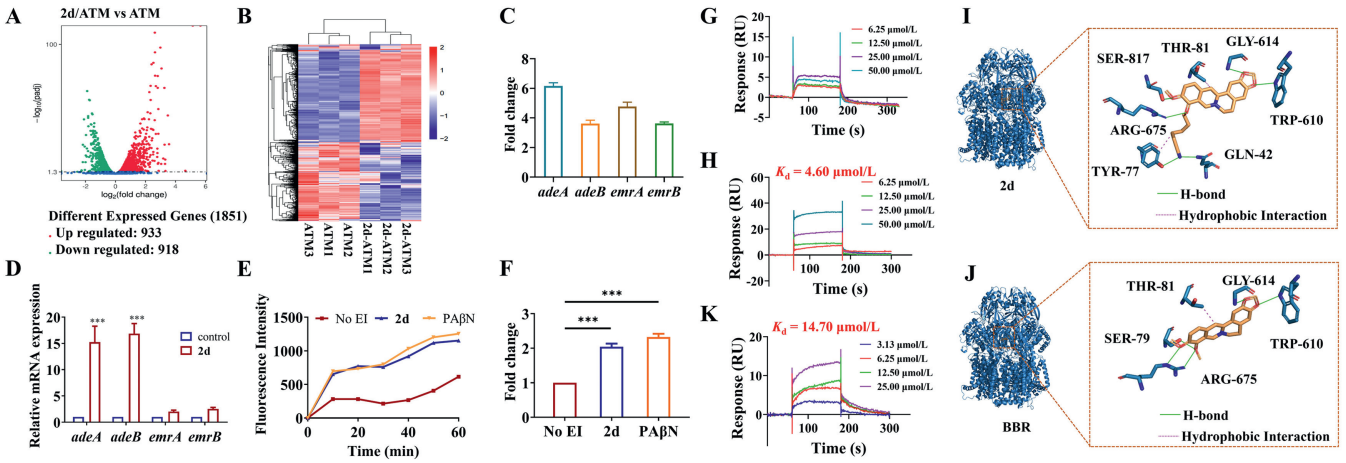

Fig. 2. Target proteins analysis and verification. (A) Volcano plot and (B) Heatmap analysis of the differential expression genes in *A. baumannii* after exposing the combination of ATM (4 μg/mL) plus **2d** (4 μg/mL) or ATM (4 μg/mL). (C) The up-regulation of efflux-pump related genes of **2d** and ATM (4 and 4 μg/mL)-treated *A. baumannii* in comparison to ATM (4 μg/mL) in transcriptome analysis. (D) Quantification of efflux pump genes expression normalized with control (ATM 4 μg/mL). ATM and **2d** were added at 4 and 4 μg/mL for 4 h. (E) The relative fluorescence intensity of ethidium bromide in *A. baumannii* ATCC 19606 with the treatment of **2d** and PAβN during 60 min incubation. (F) The fold change of relative fluorescence intensity of ethidium bromide in *A. baumannii* ATCC 19606 with treatment of **2d** and PAβN strain at 60 min post incubation. (G) SPR sensorgrams obtained on a purified AdeA-coated chip at different concentrations of **2d**. (H) SPR sensorgrams obtained on an AdeB fragment-coated chip at different concentrations of **2d**. (I) Molecular docking for AdeB (PDB code: 6OWS) with **2d**. (J) Molecular docking for AdeB (PDB code: 6OWS) with BBR. (K) SPR sensorgrams obtained on an AdeB fragment-coated chip at different concentrations of BBR. Values are mean ± standard deviation (SD) ($n = 3$). $^{***}P < 0.001$.

pound **2d** increased the susceptibility of *A. baumannii* to all evaluated antibacterial. The addition of **2d** at concentrations of 64–128 μg/mL significantly lowered the inhibitory concentrations of MEM, AMI, CIP, CPM, CAP and SUL to 1/4 of their respective MICs (Table S6). The degree of combination responses was further analyzed and visualized by the online SynergyFinder software using zero interaction potency (ZIP) calculation method [27]. As depicted in Fig. S1 (Supporting information), the ZIP scores of **2d** with various antibacterial agents, including ATM, MEM, AMI, CIP, CPM, CAP and SUL were 20.011, 15.605, 10.143, 13.891, 12.343, 8.496 and 12.602, respectively (ZIP score: >0 indicated synergy; >10 indicated strong synergy). These findings showed that compound **2d** demonstrated highly synergistic effects when combined with the tested antibacterial against *A. baumannii*.

Galleria mellonella (*G. mellonella*) larvae have emerged as a reliable and commercially available model for studying the *in vivo* efficacy of antimicrobial agents against pathogen infections [28]. To investigate the protective effect of the **2d**/ATM combination against *A. baumannii* infection, *in vivo* experiments were conducted using *G. mellonella* larvae. The larvae were challenged a lethal dose of 1×10^6 colony-forming units (CFU) of *A. baumannii* ATCC 19606, and treated with a single injection of 10 μL of phosphate buffer saline (PBS), 8.3 mg/kg **2d**, 66.7 mg/kg ATM, or **2d** and ATM (8.3 and 66.7 mg/kg) 0.5 h post-infection. As depicted in Fig. 1D, most larvae treated with PBS, **2d** or ATM alone succumbed to the infection within 48 h of *A. baumannii* inoculation. Notably, the monotherapy of either compound failed to provide protection against the lethal infection. However, the combination of **2d** and ATM showed a significant increase in the survival rate, with 80% of the larvae surviving up to 96 h post-infection. The survival rate was significantly higher in the combination group compared to the monotherapy groups ($P < 0.01$). Thus, the **2d** and ATM combination exhibited potent protective efficacy against lethal *A. baumannii* infection.

To facilitate and visualize the evaluation of anti-*A. baumannii* adjuvant candidates, a stable autoluminescent ESBL-producing *A. baumannii* strain UAlAb was employed for potency study both *in vitro* and *in vivo*. As shown in Fig. 1E, the triple-combination of **2d** (32 μg/mL) with ATM and AVI (4 and 2 μg/mL) exhibited significantly synergistic effect against *A. baumannii* UAlAb in checkerboard assay as demonstrated by bioluminescent monitoring. In the *G. mellonella* larvae model, the control group of infected larvae displayed the strongest luminescence at 24 h post-infection and eventually all died as displayed in Figs. 1F and G. The ATM/AVI group showed partial protection, with 3 out of 5 larvae developing varying degrees of luminescence at 24 h post-infection but ultimately all succumbing to the infection by 72 h (Figs. 1F and H). Meanwhile, the **2d**/AVI/ATM triple-combination group showed minimal luminescence at 24 h post-infection (Fig. 1I), and had a significantly better protective efficacy, with 4 out of 5 larvae (80%) surviving at 96 h, compared to the ATM/AVI group (Figs. 1F and I). Therefore, the luminescence intensity of infected larvae at 24 h post-infection can serve as a valuable indicator of the protective efficacy.

To gain insight into the synergic mechanism of **2d**, transcriptome analysis of *A. baumannii* ATCC 19606 exposure to ATM alone and in combination with **2d** was performed. After co-cultured with ATM (4 μg/mL) for 2 h, the bacteria were treated with or without **2d** at the concentration of 4 μg/mL for 4 h. The comparison of treatment with **2d**/ATM combination to ATM alone revealed an up-regulation of 983 and down-regulation of 918 differentially expressed genes (Figs. 2A and B). Notably, the results revealed that the transcriptional levels of four efflux-pump coding genes, including *adeA*, *adeB*, *emrA* and *emrB*, were significantly up-regulated (Fig. 2C). This suggested that the possible suppression of the efflux-pump system by **2d** led to a compensatory transcriptional up-regulation of the corresponding efflux-pump related genes. Next, the differential gene expression analysis was verified using quantitative PCR (RT-qPCR) assay. As depicted in Fig. 2D, the expression changes of *adeB* and *adeA* were more significant than those of *emrA* and *emrB* in *A. baumannii* ATCC 19606 between ATM/**2d** treatment group and ATM group. Antibiotic efflux is one of the major resistant mechanisms, whereby bacteria pump out the antibiotics from their cellular interior to the external environment using special transporter proteins called efflux pumps. It has gained significant attention in the discovery and optimization of synthetic and naturally derived efflux pump inhibitors (EPIs) in the past two decades. EPIs can provide an available option to restore the pharmacological activity and clinical efficacy of some first-line antibiotics.

The capacity of **2d** to impede the efflux of ethidium bromide, a recognized substrate of the efflux pump, from *A. baumannii* was

subjected to further assessment utilizing a fluorescence-based assay. The fluorescence intensity of ethidium bromide experiences enhancement upon its interaction with bacterial DNA. As depicted in Figs. 2E and F, a notable increase in fluorescence was observed in the presence of **2d** or PAβN, a widely recognized inhibitor of efflux pumps. This increase in fluorescence signifies a pronounced inhibition on the efflux of ethidium bromide, in comparison to the untreated control group. When *A. baumannii* was treated with **2d** or PAβN, there emerged an elevation of approximately 2.04- and 2.32-fold in the fluorescence intensity of ethidium bromide, respectively, compared with the untreated control following a 60-min incubation. These findings collectively suggest that **2d** likely hindered the efflux of ethidium bromide by rendering the bacterial efflux pumps inactive.

As one of the best studied efflux pumps, the resistance-nodulation-division (RND) family-type pump AdeABC was reported to be expressed in an estimated 80% of clinically isolated *A. baumannii* strains and has a broad substrate range. Similar to other RND-type pumps, AdeABC has a three-component structure: membrane fusion protein (AdeA), inner membrane efflux transporter (AdeB), and outer membrane protein (AdeC) [29]. Also, confocal analysis demonstrated that **2d** could enter *A. baumannii* (Fig. S2 in Supporting information). Thus, according to the RT-qPCR results, recombinant AdeA and AdeB proteins were expressed and purified. The affinity with **2d** was then evaluated through surface plasmon resonance (SPR) assay. As depicted in Figs. 2G and H, **2d** could directly bind to immobilized AdeB fragment protein in a concentration-dependent manner, with a K_d value of 4.60 μmol/L, while **2d** had no interaction with the AdeA protein, suggesting a possible interaction between **2d** and AdeB.

The importance of the proximal multidrug binding site for AdeB activity has been established, as evidenced by the conservation of residues in the F and G loops among other multidrug pumps, such as AcrB and MtrD. To investigate the interaction between AdeB and **2d**, molecular dockings were carried out, with BBR serving as a control. The G-loop residues of AdeB, which are ^{609}GWGFSGA^{615}, were chosen as the docking sites. As shown in Figs. 2I and J, compound **2d** gave the affinity score of −8.3 kcal/mol, while BBR gave the score of −8.1 kcal/mol (affinity score < −7.0 kcal/mol was considered a strong interaction between protein and ligand; −7.0 kcal/mol < affinity score < −5.0 kcal/mol was considered good interaction; affinity score > −5.0 kcal/mol indicated a certain interaction) [30]. The molecular docking results indicate that both compounds fit well in the G-loop, forming three hydrogen bonds with the TRP610, GLY614 and ARG675. In addition, compound **2d** also formed three more hydrogen bonds interactions with the GLN42, TYR77 and SER817, as well as hydrophobic interactions with THR81 and TYR77, which might contribute to its higher affinity. Molecular dynamics simulation analysis of **2d** further demonstrated that the binding status was stable, and again verified the possible hydrogen bonds interactions between **2d** and AdeB (Fig. S3 in Supporting information).

Additionally, the affinity between BBR and AdeB was also evaluated using SPR assay, and the K_d value was 14.73 μmol/L (Fig. 2K), while **2d** gave the K_d value of 4.60 μmol/L (Fig. 2H). Our results verified that **2d** had a stronger interaction affinity with AdeB, compared with that of BBR, indicating that **2d** may be a potent inhibitor of the multidrug transporter AdeB. By preventing the efflux effect of structurally diverse antibiotics, **2d** could potentially achieve a synergistic antimicrobial effect.

On account of the observed interaction between **2d** and AdeB, the genotype of both the standard and clinically isolated strains utilized in the synergistic study was investigated by PCR. The strains demonstrated synergistic effects between **2d** and ATM were found to harbor the *adeB* gene (Fig. 3A). In contrast, the other three strains (21-2, 21-5, 21-16) displayed no synergy in the checkerboard assay were lack of *adeB* gene. These results again substantiate the ability of compound **2d** to augment the antibacterial efficacy of ATM against strains that produce AdeB.

To further elucidate whether the action of **2d** on drug efflux is specifically targeted at AdeB, an *adeB*-overexpressing strain, 19606-p-*adeB*, was constructed. Validation of *adeB* gene overexpression was ascertained by comparing the PCR amplification products of the extracted plasmids (Fig. 3B) and the gene transcription levels (Fig. 3C) of both the parental strain (ATCC 19606) and the mutant counterpart (19606-p-*adeB*). Given that the *adeB* gene in ATCC 19606 is solely located in the chromosome, no 675 bp band was amplified from the extracted plasmid of the wild-type strain. Conversely, amplified PCR products of *adeB* from the plasmid and a 7.00 ± 0.97-fold increase in mRNA expression level were observed in the overexpressing strain. Subsequently, a checkerboard assay was conducted utilizing the 19606-p-*adeB* strain, compared with the parental strain. As depicted in Table S7 (Supporting information), the MIC value of ATM increased from 32 μg/mL to 64 μg/mL in the 19606-p-*adeB* strain. Additionally, the presence of **2d** at 4 μg/mL, which exhibited a significant synergistic effect with ATM in the wild-type strain, did not lead to a significant decrease in the MIC of ATM against the 19606-p-*adeB* strain, maintaining a value of 64 μg/mL. Therefore, no synergy was discernible between ATM and **2d** in the 19606-p-*adeB* strain at this **2d** concentration, as indicated by an FICI value of 1.003. When the concentration of **2d** was increased to 32 μg/mL and above, the synergy between **2d** and ATM was restored, with the MIC of ATM reduced to 16 μg/mL and an FICI value of 0.282. This observation implies that the overproduction of AdeB makes **2d** unable to completely occupy all active sites of the AdeB protein, thus preventing the efflux of ATM.

In addition to the efflux pump system, transcriptome analysis showed significant up-regulation of genes related to iron acquisition (Fig. 3D), indicating that the administration of **2d** may inhibit iron acquisition in *A. baumannii*. Specifically, the transcriptional level of acinetobactin (Aci) receptor BauA-coding gene *bauA* was significantly up-regulated, suggesting that the recycling of Aci in *A. baumannii* might be suppressed. Iron is a trace element that is essential for nearly all bacterial pathogens. However, the level of free iron at the host-pathogen interface is magnitude below what is required to support the microbial growth. To counteract iron starvation, bacteria have developed several iron acquisition strategies, including the secretion of iron-binding small molecules known as "siderophores" to steal iron from transferrin and lactoferrin. Aci is often identified as the major siderophore produced by *A. baumannii,* but it is still unclear how Aci is pumped out extracellularly.

As depicted in Fig. 3E, the iron deficiency state (indicated by the dark blue curve) of bacteria can be reversed through adding plasma (purple curve). However, the growth of bacteria in plasma can be then inhibited in a dose-dependent manner upon the addition of **2d** (4 μg/mL in red and 200 μg/mL in green curve). In this case, the growth of bacteria could be restored upon the complementary addition of Aci (orange and cyan curve). These results indicate that after the administration of **2d**, the amount of Aci excreted by bacteria is insufficient, leading to growth inhibition. The addition of exogenous Aci can reverse the growth inhibition of bacteria caused by **2d**.

Based on a previous report, the expression of AdeB was increased more than four-fold under low iron conditions (20 μmol/L). We speculate that Aci is exported to the extracellular space through AdeABC pump for capturing Fe(III) from the host. The complex was then taken back into the pathogens by the receptor protein (BauA). After the addition of **2d**, it inactivated the AdeABC efflux pump system, and then suppressed the export of Aci and the subsequent iron uptake of *A. baumannii*. As shown in Figs. 3F and G, Aci could formed a stable and colored 2:1 complex with Fe(III). SPR experiment also showed that Aci displayed a strong affinity

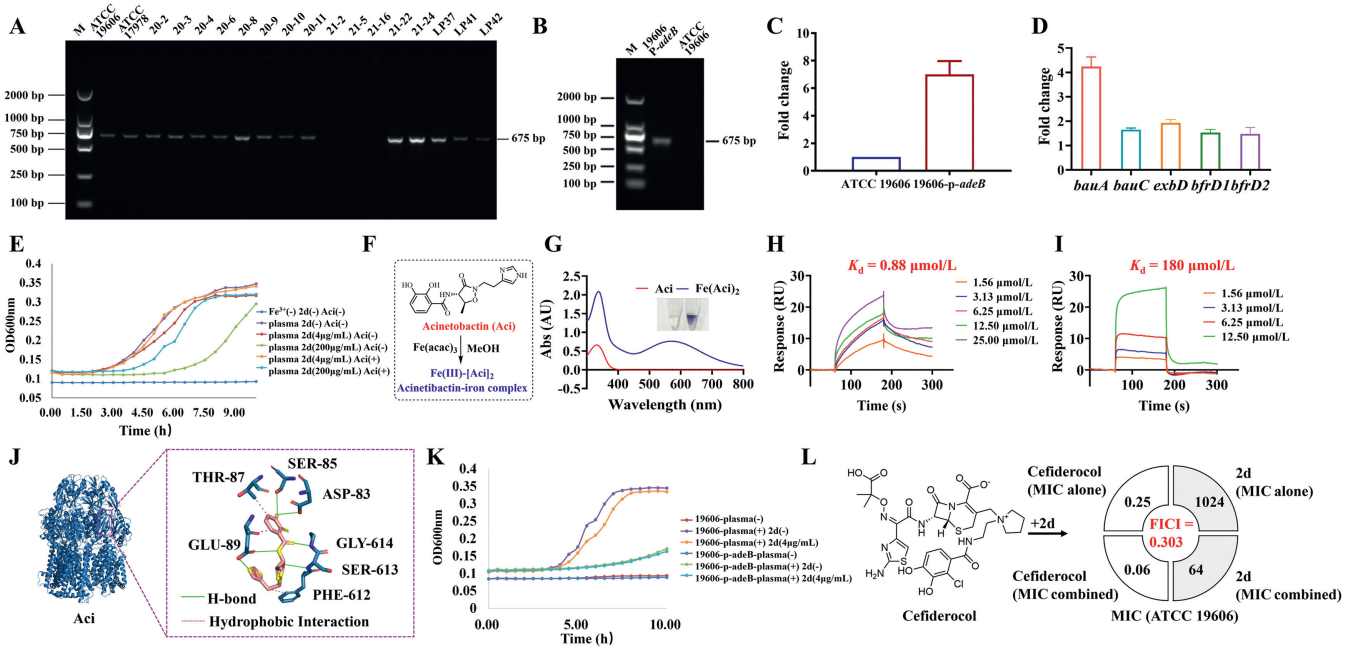

Fig. 3. The influence on iron uptake by the interaction of compound **2d** and AdeB protein. (A) Electrophoresis of PCR products of standard and clinical isolated *A. baumannii* strains, designing to verify the existence of *adeB* gene. Lane 1, molecular weight marker. Lanes 2 and 19, PCR products obtained from standard strains and clinical isolates. (B) Electrophoresis of PCR products of the extracted plasmids from mutant strain 19606-p-*adeB* and *A. baumannii* ATCC 19606 wild type. (C) Quantification of *adeB* gene expression levels. (D) Changes in transcriptional levels of iron uptake related genes of **2d** and ATM (4 and 4 μg/mL)-treated *A. baumannii* in comparison to the ATM (4 μg/mL) group. (E) Growth curve of *A. baumannii* ATCC 19606 in M9 iron deficient media as measured at OD_{600}. (F) Structure of acinetobactin (Aci) and synthesis of Fe(III)-$[Aci]_2$. (G) Ultraviolet–visible spectrophotometry (UV–vis) absorption spectra of Aci (200 μmol/L) and Fe(III)-$[Aci]_2$ (200 μmol/L) in HEPES (1 mol/L, pH 7.4). SPR sensorgrams obtained on a purified AdeB fragment-coated chip at different concentrations of (H) Aci or (I) Fe(III)-$[Aci]_2$. (J) Molecular docking for AdeB (PDB code: 6OWS) with Aci. (K) Growth curve of AdeB overexpressing and wild-type *A. baumannii* 19606 strains in M9 iron deficient media as measured at OD_{600}. (L) Structure of cefiderocol and results of checkerboard assay for **2d**/cefiderocol combination against *A. baumannii* ATCC 19606. Values are mean ± SD ($n = 3$).

binding with immobilized AdeB fragment protein with a K_d value of 0.88 μmol/L, while Fe(III)-$[Aci]_2$ gave a K_d value of 180 μmol/L, which further confirmed that AdeABC might be the efflux channel of Aci (Figs. 3H and I). The molecular docking analysis between Aci and AdeB protein was then performed. As shown in Fig. 3J, Aci could fit well in the active pocket of AdeB, where six hydrogen bonds and three hydrophobic interactions contributed together to their strong interactions, with an affinity score of −7.7 kcal/mol. It is worth noting that the addition of **2d** showed no obvious inhibitory effect on the growth of 19606-p-*adeB* strain (green curve and cyan curve, Fig. 3K), indicating that the overexpression of AdeB might compensate for the restriction of iron acquisition and bacterial growth caused by **2d**. Compared with the parental strain, the relatively slow growth rate of the 19606-p-*adeB* strain can be explained by the fitness cost effect after receiving the *adeB* overexpressing plasmid.

Cefiderocol is a novel siderophore cephalosporin conjugated with a catechol moiety, with a promising *in vitro* and *in vivo* activity against *A. baumannii* [31]. It was approved by the U.S. Food and Drug Administration (FDA) in 2019 to treat hospital-acquired pneumonia and ventilator-associated pneumonia caused by *A. baumannii*. Cefiderocol binds to Fe(III) and is actively transported into bacteria through bacterial iron transporter and outer membrane. A study conducted with Hua *et al.* in 2023 showed that a combination of cefiderocol and CCCP, as an efflux pump inhibitor, has synergistic effect on infections caused by *A. baumannii* isolates [32]. We further verified the synergistic effect between **2d** and cefiderocol against *A. baumannii* ATCC 19606 (Fig. 3L). The MIC of cefiderocol against *A. baumannii* was reduced from 0.25 μg/mL to 0.06 μg/mL with the addition of 64 μg/mL **2d**. The synergic effect of **2d** to cefiderocol might attribute to its suppressive effects on both iron uptake and efflux pump, leading to the increasing concentration of cefiderocol inside the bacteria. These data suggested that **2d** could facilitate antibiotic efficacy by competing against antibiotics and Aci for the binding sites of AdeB, thus increasing the antibiotic uptake and the susceptibility against *A. baumannii* (Fig. 4).

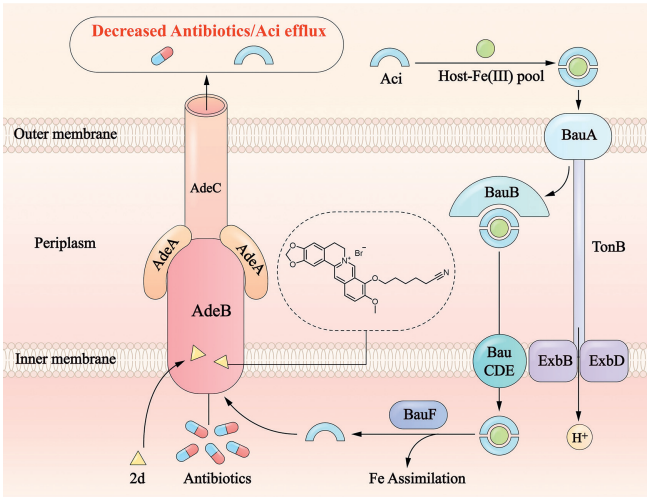

Fig. 4. Proposed model for potentiating mechanism of **2d** against *A. baumannii* highlighting the antibiotic efflux and iron acquisition function of AdeB.

To summarize, this study designed, synthesized, and evaluated thirty novel BBR derivatives for their synergistic antibacterial activity against *A. baumannii*. Among these derivatives, compound **2d** demonstrated the most promising synergetic potency, decreasing the MIC value of ATM to no more than 1/4 of its MIC when used alone, which was superior to that of BBR. Instead of killing

the bacteria itself, compound **2d** could exert its synergistic effect on the effectiveness of ATM by the reducing the efflux of ATM and enhancing ATM's concentration in bacteria. Compound **2d** also demonstrated *in vitro* synergistic effects against CRAB strains and ESBLs producing strains in dual- and triple- combinations, respectively. In *G. mellonella* larvae model, **2d**/ATM combination could significantly increase the survival rate of the larvae compared to either component alone. Mechanism study disclosed that **2d** might inhibit the efflux pump and iron acquisition of *A. baumannii* by binding to AdeB, thereby achieving synergistic antimicrobial efficacy (Fig. 4). Our study provides instructive guidance for the further development of BBR derivatives as anti-*A. baumannii* antibiotic adjuvants with a dual-function antibacterial mechanism.

Declaration of competing interest

The authors declare that they have no known competing financial interests or personal relationships that could have appeared to influence the work reported in this paper.

Acknowledgments

We appreciate Dr. Tianyu Zhang (Guangzhou Institutes of Biomedicine and Health, Chinese Academy of Sciences) for kindly providing the autoluminescent *Acinetobacter baumannii* strain UAlAb. This research project was supported by grants from National Natural Science Foundation of China (Nos. 32141003, 82104013), and CAMS Initiative for Innovative Medicine (Nos. 2021-1-I2M-070, 2021-1-I2M-039, China).

Supplementary materials

Supplementary material associated with this article can be found, in the online version, at doi:10.1016/j.cclet.2024.109506.

References

[1] E.S. Milani, A. Hasani, M. Varschochi, et al., J. Hosp. Infect. 117 (2021) 135–146.
[2] T. Demirdal, U.S. Sari, S.A. Nemli, Ann. Clin. Microbiol. Antimicrob. 15 (2016) 11–17.
[3] O. Ayobami, N. Willrich, T. Harder, et al., Emerg. Microbes Infect. 8 (2019) 1747–1759.
[4] S. Domingues, N. Rosário, Â. Cândido, et al., Microorganisms 7 (2019) 30–37.
[5] W.P. Xu, Z. Ma, G. Dhanda, et al., Chin. Chem. Lett. 34 (2023) 107847.
[6] C. Willyard, Nature 543 (2017) 15.
[7] G.D. Wright, Trends Microbiol. 24 (2016) 928.
[8] E.E. Gill, O.L. Franco, E.W. Hancock Robert, Chem. Biol. Drug Des. 85 (2014) 56–78.
[9] L. Kalan, G.D. Wright, Expert. Rev. Mol. Med. 13 (2011) e5.
[10] Y. Chen, Z. Li, Y. Yin, et al., Chin. Chem. Lett. 34 (2023) 107948.
[11] C.F. Liu, Z.X. Li, H. Yu, et al., Chin. Chem. Lett. 32 (2021) 1385–1389.
[12] Q.X. Zeng, W. Wei, T. Fan, et al., CCS Chem. 4 (2022) 1535.
[13] W. Wei, Q.X. Zeng, Y. Wang, et al., Acta Pharm. Sin. B 13 (2023) 2138–2151.
[14] M. Tillhon, L.M. Guamán Ortiz, P. Lombardi, et al., Biochem. Pharmacol. 84 (2012) 1260–1267.
[15] X. Li, Y. Song, L. Wang, et al., Front. Cell Infect. Microbiol. 11 (2021) 660431.
[16] H. Yao, L. Cui, H. Liu, et al., Chin. Chem. Lett. 35 (2024) 108511.
[17] G. Chen, L.R. Swem, D.L. Swem, et al., Mol. Cell 42 (2011) 199–209.
[18] T.L. Harris, R.J. Worthington, L.E. Hittle, et al., ACS Chem. Biol. 9 (2014) 122–127.
[19] J. Sianturi, P. Priegue, J. Hu, et al., Angew. Chem. Int. Ed. 61 (2022) e202209556.
[20] S. Siricilla, K. Mitachi, J. Yang, et al., J. Med. Chem. 60 (2017) 2869–2878.
[21] A. Hammad, N.S. Abutaleb, M.M. Elsebaei, et al., J. Med. Chem. 62 (2019) 7998–8010.
[22] H. Sun, M.F. Ansari, N. Battini, et al., Org. Chem. Front. 6 (2019) 319–334.
[23] T.Y. Fan, Y.X. Wang, S. Tang, et al., Eur. J. Med. Chem. 157 (2018) 877–886.
[24] G.B. Zhang, S.K. Maddili, V.K.R. Tangadanchu, et al., Sci. China Chem. 61 (2017) 557–568.
[25] W.W. Gao, L. Gopala, R.R.Y. Bheemanaboina, et al., Eur. J. Med. Chem. 146 (2018) 15–37.
[26] L. Di, E.H. Kerns, Hong Y, et al., Int. J. Pharm. 297 (2005) 110–119.
[27] A. Ianevski, A.K. Giri, T. Aittokallio, Nucl. Acids Res. 48 (2020) W488–W493.
[28] Y. Tao, L. Duma, Y. Rossez, Pathogens 10 (2021) 1483.
[29] M. Zwama, K. Nishino, Antibiotics 10 (2021) 774.
[30] K.Y. Hsin, S. Ghosh, H. Kitano, PLoS One 8 (2013) e83922.
[31] M. Kollef, H. Dupont, D.E. Greenberg, et al., Int. J. Antimicrob. Agents 62 (2023) 106882.
[32] X.C. Liu, Y.J. Chang, Q.Y. Xu, et al., mSystems 8 (2023) e0129122.